*Int. J. Electrochem. Sci.*, 8 **(2013)** 9000 - 9014

International Journal of
ELECTROCHEMICAL
SCIENCE
www.electrochemsci.org

# Surface and Bulk Properties of $LiFePO_4$ Probed by the Magnetic Analysis

*K. Zaghib*[1], *J. Trottier*[1], *A. Mauger*[2], *H. Groult*[3], *C. M. Julien*[3,*]

[1]Energy Storage and Conversion, Hydro-Québec Research Institute, 1800 Boul. Lionel-Boulet, Varennes, QC, Canada, J3X 1S1
[2]Université Pierre et Marie Curie-Paris6, IMPMC, 4 Place Jussieu, 75252 Paris Cedex 05, France
[3] Université Pierre et Marie Curie-Paris6, PECSA, UMR7195, 4 Place Jussieu, 75005 Paris, France
[*]E-mail: christian.julien@upmc.fr

*Received:* 28 April 2012 / *Accepted:* 24 April 2013 / *Published:* 1 July 2013

The electrochemical properties of $LiFePO_4$ are not only governed by the structural homogeneity of the bulk material but also by the surface condition of each primary particle. The magnetic properties of $LiFePO_4$ particles probing both bulk and surface are reviewed. Their analysis is a very efficient tool of characterization of the intrinsic properties of the bulk material. They are also used to identify and determine the concentration of the impurities and of the defects, separately. They are also used to characterize the surface layer, study its crystallinity, and its delithiation upon exposure to moisture. The electrochemical features of 40-nm sized $LiFePO_4$ particles before carbon coating and after carbon-coating are tested in $LiFePO_4$/$LiPF_6$-EC-DEC/Li cells.

**Keywords:** Olivine; Magnetic properties; Cathode materials; Li-ion batteries

## 1. INTRODUCTION

The research and development of Li-ion batteries have played a major role in our way of life and in the world economy. First limited to portable use, the recent progress now makes possible the use of such batteries for electric vehicles. In this context, $LiFePO_4$ cathode is the winner. Its theoretical capacity 160 mAh/g is close to its theoretical value. The energy density is large enough to insure autonomy of 200 miles (even more) for the electric cars that are commercialized in different countries [1]. The safety is remarkable, the power is high, and allows for a fast charge process with an outstanding cycling life, since full capacity is maintained after 30 000 cycles with the appropriate anode [2]. First proposed by Padhi et *al.* [3], the material suffered from different problems that had to be solved, starting with a low electronic conductivity. The coating of the particles with conductive

carbon has solved this problem [4]. Then, it was necessary to remove the impurities. Then the investigation of intrinsic properties was needed to determine the key parameters that control the electrochemical performance and optimize them. It was also needed to control the surface layer that is important for small particles. All these steps demanded careful characterization of the materials, and the success of the Li-ion batteries is primarily that of material sciences.

The cathode elements of Li-ion batteries are oxides of transition metal. The transition metal ions carry a magnetic moment (except $Co^{3+}$), so that the analysis of the response of the moment to a magnetic excitation gives access to its local environment. The analysis of the magnetic properties is thus a tool to characterize these materials at the atomic scale, with a remarkable sensitivity. We have previously reviewed such an analysis in the case of lamellar compounds [5]. We report hereunder this analysis in the case of $LiFePO_4$. The different synthesis approaches, and the more conventional means of characterization of this material have been reviewed in [6] and [7], respectively, so that the present work is strictly focused on the magnetic properties to promote magnetism as a tool for the research in Li-ion batteries.

## 2. EXPERIMENTAL

Submicron-sized powders were prepared by hydrothermal route assisted by complexing agent. We used $FeSO_4 \bullet 7H_2O$, $H_3PO_4$ and $LiOH \bullet H_2O$ as chemical precursors. Attention has been taken to choose the proportion of the precursors corresponding to stoichiometry. We have investigated elsewhere the consequence of a departure from stoichiometry. The Li deficiency in the preparation process results in a partial occupation of Li sites by Fe, forming the defect $Fe^{\bullet}_{Li} + V'_{Li}$ in the Kröker-Vink notation. Therefore, the chemical formula switches to $Li_{1-2x}Fe_xFePO_4$ or, in closed form, $Li_{1-2x}Fe_{1+x}PO_4$. This defect has also been observed in samples synthesized by hydrothermal at temperature below 200 °C. The carbon coating was achieved using the lactose method: the particles were mixed with the carbon precursor (lactose) in acetone solution. The nominal dry additive corresponded to 5 wt.% carbon in $LiFePO_4$. After drying, the blend was heated at 650 °C for 2 h in an inert atmosphere. The final quantity of carbon was about 2 wt.% of the material (Cdetector, LECO Co., CS 444). This process leads to a homogeneous, 3 nm-thick surface layer of conductive carbon.

For morphological analysis, a transmission electron microscopy (TEM) study of the samples was performed using a Hitachi (Japan) electron microscope. The magnetic measurements (susceptibility and magnetization) were performed with two fully automated SQUID magnetometer (Quantum Design MPMS-5S) in the temperature range 4–300 K.

The electrochemical properties were tested at room temperature in cells with metallic lithium as anode electrode. Charge–discharge tests were performed on coin type cell (CR2032). Composite positive electrode was prepared by thoroughly mixing the active material (90 wt%) with carbon black (2 wt.%), acetylene black (2 wt.%), polyvinylidene fluoride (6 wt.%) in N-methyl-pyrrolidinone and spread onto aluminium foils then dried for 24 h at 120 °C in vacuum. Cathode loading was 9 $mg/cm^2$. Cells were then assembled in an argon-filled glove box using foils of Li metal as counter electrode and Celgard 2400 as separator. The electrolyte was 1.0 $mol.L^{-1}$ $LiPF_6$ in a mixture of ethylene carbonate

(EC) and diethyl carbonate (DEC) (1:1, v/v). The cells were galvanostatically cycled between 2.2 V and 4.0 V versus $Li^+$/Li on a Mac-Pile battery tester at room temperature.

## 3. RESULTS AND DISCUSSIONS

### *3.1. Intrinsic magnetic properties*

Well-crystallized $LiFePO_4$ is antiferromagnetic (AF), with a Néel temperature $T_N$=52 K [8]. In the absence of impurities, the magnetic properties are very simple: the magnetization versus magnetic field is linear at any temperature up to the highest field available in the experiments (30 kOe), so that the magnetic susceptibility is $\chi=M/H$ with $M$ the magnetization measured in any field.

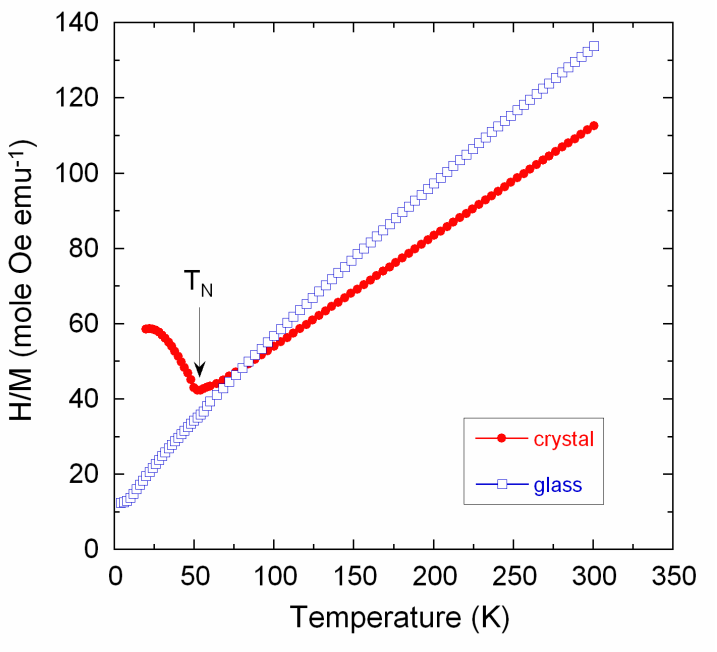


**Figure 1**. Temperature dependence of the reciprocal magnetic susceptibility of well-crystallized and of amorphous $LiFePO_4$. The cusp at the Néel temperature $T_N$=52 K is observed only in the well-crystallized sample.

Figure 1 illustrates the $\chi^{-1}(T)$ curve for a sample in which no impurity effect has been detected (the impurity effects will be described in a forthcoming section). The cusp at $T_N$ characterizes the antiferromagnetic ordering. The topology of the AF order has been determined by neutron diffraction [9], from which the magnetic interactions have been determined [10]. The dominant interactions that fully account for this structure are the intralayer superexchange Fe-O-Fe interaction $J_1$, and two Fe-O•••O-Fe superexchange interactions, namely an interlayer interaction $J_2$ and an intralayer interaction $J_b$. Other interactions [11] turn out to be negligible. All these interactions $J_1$, $J_2$ and $J_b$ are antiferromagnetic. The paramagnetic Curie temperature deduced from the fit of the $\chi^{-1}(T)$ curve by the

Curie-Weiss law $\chi(T) = C/(T+\theta)$ in the paramagnetic region is $|\theta| \sim 110$ K. The effective magnetic momentum $\mu_{eff}$ carried by the $Fe^{2+}$ ions deduced from the Curie Constant $C$ is $\mu_{eff} = 4.9\ \mu_B$ for the best samples without impurity or defect in it. This is in quantitative agreement with the value expected for $Fe^{2+}$ in the high-spin state $S$=2. Incidentally, it shows that the orbital momentum is fully quenched [12]. This is a feature that is not specific to $LiFePO_4$, as it is in common with many cathode elements [13]. The reason is that these materials are ionic, so that the cations and anions carry an electric charge that is not screened like in semiconductors or metals where the dielectric constant is much larger. As a consequence the Coulomb (crystal field) interactions are strong. Since the orbital contribution due to the magnetic moment is of second order in perturbation with respect to the crystal field, this contribution is scaled by the square of the ratio between the spin-orbit and the crystal field interaction, which explains that it is negligible.

So far, we have displayed the intrinsic magnetic properties for well-crystallized samples. In $LiFePO_4$ glasses, however, no cusp in the susceptibility curve has been observed [14-15], as is also shown in Fig. 1. The extension of the spin correlation function in this case is restricted to the mean distance between structural defects, which is only the order of the nanometer in glasses. This feature prevents the spatial extension of the spin correlation function upon cooling to propagate the AF order at long range; a true antiferromagnetic phase transition requires the divergence of spin correlation length at $T_N$ (in practice a spin correlation length large compared to the distance between magnetic ions). The long-range antiferromagnetic ordering can also be impeded by the presence of local defects. In that case, the extension of the spin correlation length is limited not to the lattice coherence length, as in a glass, but to the distance between defects. We have met this situation in samples obtained at the very early stage of synthesis by solid-state reaction, *i.e.* sintered at $T_s$= 300 °C only [16]. In that case, XRD peaks showed that the $LiFePO_4$ phase had already grown, but the temperature was just too low to get rid of the impurities and defects. As a consequence, the observation of the cusp of the magnetic susceptibility at $T_N$ already indicates that the sample is crystallized with a coherence length that is large compared with the lattice parameter. However, XRD is required to determine quantitatively this coherence length by using the Scherrer law. On another hand, any deviation of $\mu_{eff}$ from 4.9, and any deviation of $M(H)$ from linearity will mean the presence of impurities and defects. This case is illustrated in the next section.

### *3.2. Impurities*

Different clustering effects have been found depending on the synthesis parameters used to prepare the materials. A firing temperature larger than 800 °C increases the fraction of $Fe_2P$ [17], but $Fe_2P$ nano-particles large enough to be superparamagnetic have been detected in samples that have not been heated to such high temperatures [18]. On one hand, the presence of $Fe_2P$ can increase the electronic conductivity, but on another hand it also decreases the ionic conductivity so that both the capacity and cycling rates are degraded with respect to the carbon-coated $LiFePO_4$. In addition, $Fe_2P$ also has the disadvantage that it dissolves in the electrolyte, leading to the migration of iron to the anode of the Li-ion battery. It is thus imperative to get rid of this impurity. Another impurity that must

be avoided is γ-$Fe_2O_3$ that could be found under certain conditions under the form of a small concentration ($1.0\times10^{-6}$ per chemical formula) of γ-$Fe_2O_3$ nanoparticles [18-19].

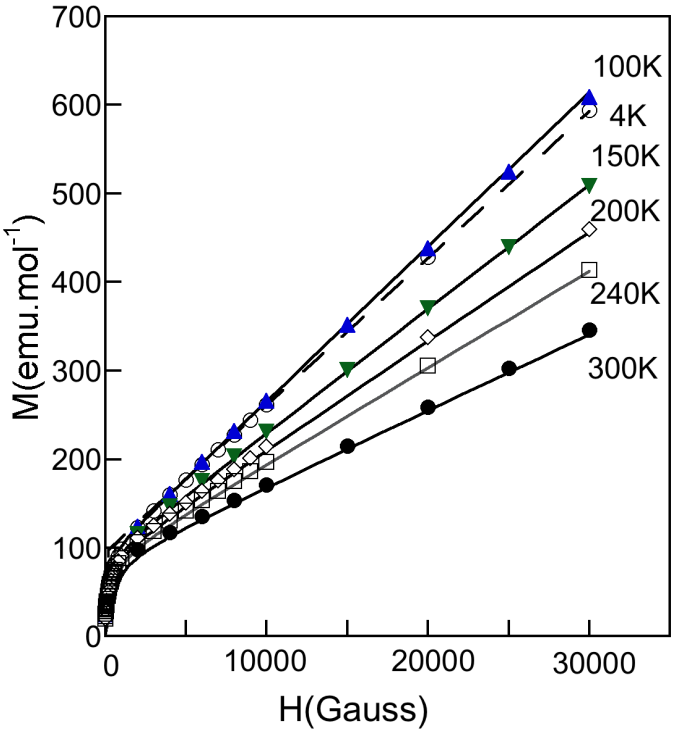


**Figure 2**. Isothermal curves of the magnetic moment vs. applied magnetic field as a function of temperature for a sample containing γ-$Fe_2O_3$. The symbols are experimental data and the full lines are theoretical fits according to Eqs. 1-2.

Figure 2 shows the isothermal plots of the magnetic moment versus applied magnetic field for a sample containing impurities. The non-linearity of the $M(H)$ curves is a signature of ferromagnetic impurities [18-20]. The magnetization $M(H)$ is the superposition of two contributions

$$M(H)=\chi_m H+M^{extrin}, \quad (1)$$

$$M^{extrin}=Nn\mu £(\xi). \quad (2)$$

The intrinsic part, $\chi_m H$, is linear in the applied magnetic $H$, while the extrinsic component easily saturates with the application of $H$ and is due to ferromagnetic impurities. Here, $£(\xi)=£(n\mu H/k_B T)$ is the Langevin function, $N$ is the number of magnetic clusters, and each cluster is made of $n$ magnetic moments $\mu$; other notations are conventional. At high fields, $M_{extrin}$ saturates to $Nn\mu$ so that this quantity is readily determined as the ordinate at $H$=0 of the intersection of the tangent to the magnetization curves at large fields. As a result, we find that $Nn\mu$ does not depend significantly on temperature below 300 K in Fig. 2. We are in the situation where the cluster magnetization is temperature-independent, which implies that the magnetic ordering temperature $Tc$ inside the clusters

is much larger than 300 K. This feature is sufficient to identify the impurity as γ-$Fe_2O_3$ nanoparticles. Then the fit of the magnetization curves according to Eqs. 1 and 2 allows us to determine the fitting parameter $n\mu$ from which we determine $n$, since the magnetic moment per iron in γ-$Fe_2O_3$ is known. From $n$ we can deduce the size of the γ-$Fe_2O_3$ nanoparticles. Actually, the maghemite orders in a ferrimagnetic phase, so that $Tc$ is a Néel temperature rather than a Curie temperature. $\mu$ in this particular case is due to the non-compensation in the magnetic moments carried by the iron ions in the γ-$Fe_2O_3$ structure.

This hypothesis must be abandoned when the number $n$ of magnetic clusters is so large that magnetic interactions between the ferrimagnetic particles become important [18]. At high fields, $M_{extrin}$ saturates to $Nn\mu$ so that this quantity is readily determined as the ordinate at $H$=0 of the intersection of the tangent to the magnetization curves at large fields. As a result, we find that $Nn\mu$ does not depend significantly on temperature below 300 K. We are in the situation where the cluster magnetization is temperature-independent, so that the Curie temperature $Tc$ inside the clusters is much larger than 300 K. This is important information on the nature of the ferromagnetic clusters. In particular, this feature precludes the existence of $Fe_2P$ clusters in some $LiFePO_4$ samples prepared according to a different procedure [18], since the Curie temperature of $Fe_2P$ is only 220 K. The nature of the strongly ferromagnetic clusters in the present case is the signature of maghemite (γ-$Fe_2O_3$). From the value of $Nn\mu$, we find that the fraction of iron that is in embedded in the γ-$Fe_2O_3$ impurity phase is 0.3% in the present case, which is too small to be detectable by XRD. The size of the γ-$Fe_2O_3$ clusters can also be determined since the macrospin $n\mu$ can be derived from the fit of the magnetization curves at any temperature according to Eqs. 1 and 2. The result of such a fit has been reported elsewhere, showing that we are dealing with γ-$Fe_2O_3$ nanoparticles of typically 3 nm in diameter. The same procedure can be used in the case of $Fe_2P$ impurities that are identified by the Curie temperature for this material. In that case, the same type of behavior is observed at low temperature, but the quantitative fit of the magnetization curves requires that the dependence of $\mu$ with temperature is taken into account, since $Tc$= 220 K is in the temperature range explored in the experiments. An example can be found in [12, 18]. In some particular cases, the concentration of the impurity nanoparticles is so large that the magnetic interaction between them is non-negligible. In that case, Eq. 1 has been modified to take this interaction into account. The equations are more complicated, but still in closed form, and can be used to determine both the concentration of the nanoparticles and their size [18]. The magnetic experiments have thus evidenced different impurities, under the form of nanoparticles few nanometers thick, stuck at the surface of the $LiFePO_4$, even in concentration so small that they could not be detected by XRD. These nanoparticles have been observed by more recent electron microscopy experiments [21], confirming their existence that had been inferred solely from the magnetic experiments, which well illustrates the relevance of the magnetism to characterize the samples.

Other impurities can pollute this material. For instance, $Li_3Fe_2(PO_4)_3$ can also be identified by its magnetic ordering temperature even though the amount is below the threshold of detection in the FTIR spectra [16].

Of course, once these impurities could be identified, and their concentration measured quantitatively by the analysis of the magnetic properties, the synthesis parameters were modified to get rid of them. For instance, it is recommended to avoid heating $LiFePO_4$ above 750 °C to avoid the

presence of $Fe_2P$. To avoid the formation of $\gamma$-$Fe_2O_3$, and more generally the formation of any impurity involving iron in the trivalent sate, it is sufficient to add an organic material to the precursors of carbon-free $LiFePO_4$. The reason is that, upon heating, the organic compound liberates reductive gases such as hydrogen that are active kinetically to reduce $Fe^{3+}$ impurities in the 500-700 °C temperature range used [16]. The efficiency of the reduction process is also favored by the fact that the organic precursor is usually mixed with the $LiFePO_4$ chemical precursors so that the reduction occurs at a molecular scale in the course of the synthesis of the material. In addition the carbon liberated by the organic compound during the heating process coats the particles with carbon, which is required for electrochemical applications. The production of optimized samples free of impurity is always the net result of the appropriate choice of the thermal treatment, and also the careful selection of the precursors [20].

### *3.3. Li-vacancy and the magnetic polaron*

The $Li^+$ vacancy traps a $Fe^{3+}$ to insure local charge neutrality and minimize the Coulomb energy. If the defect is isolated, which is the case since in practice the concentration of Li vacancies in $LiFePO_4$ is always smaller than 1%, this $Fe^{3+}$ ion will be surrounded by $Fe^{2+}$ ions on the neighboring Fe-sites of the olivine lattice. Both the $Fe^{2+}$ and the $Fe^{3+}$ ions are in their high-spin sate, which means that each iron ion carries a localized majority-spin of moment 5 $\mu_B$. The minority-spin electrons of $Fe^{2+}$ ions have an energy above that of the majority-spin configuration [22], and the electron transfer ($Fe^{3+}$, $Fe^{2+}$)→($Fe^{2+}$, $Fe^{3+}$) between iron ions neighboring a $Li^+$ vacancy does not cost the energy of trapping by the $Li^+$ vacancy.

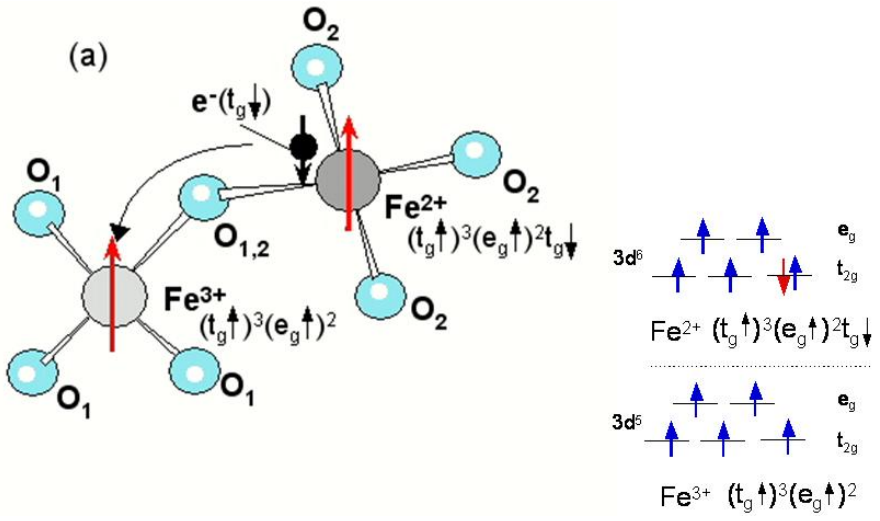


**Figure 3**. Small magnetic polaron in $LiFePO_4$ with the hopping process. The $t_g\downarrow$ "hole" on the $Fe^{3+}$ site 1 is shifted to a neighbouring iron site 2 by transfer of one $t_g\downarrow$ electron from site 2 to site 1. The indirect exchange interaction is responsible for the spin-polarization of the iron ions inside the electronic $t_g\downarrow$ "hole" wave function (in the direction opposite to that of the $t_g$ electron). As the charge in excess hops from site to site, it brings with it not only a local lattice deformation cloud associated with the Coulomb potential but also its spin-polarization cloud.

Therefore, this transfer can be fast, if the majority-spin electrons on neighboring iron are parallel to one another. A fast ($\tau_h \leq 10^{-12}$ s) hop couples ferromagnetically the cluster of iron atoms neighboring a $Li^+$ vacancy by double exchange. The $Li^+$ vacancy moves diffusively in the lattice, and the ferromagnetic cluster moves with it. The cluster of $Li^+$ vacancy and the ferromagnetically coupled iron-atom neighbors forms a magnetic polaron.

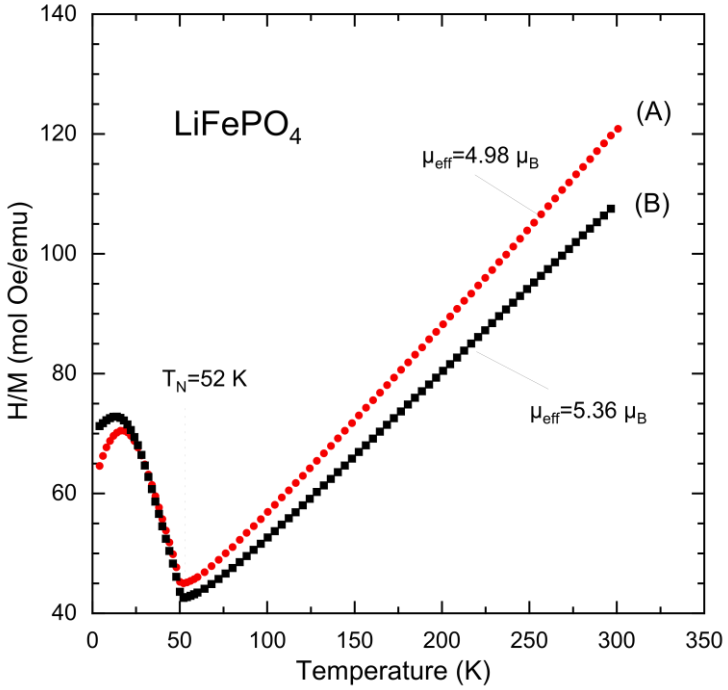


**Figure 4**. Reciprocal magnetic susceptibility of two $LiFePO_4$ samples (A) with a very small concentration of Li vacancies, (B) with a concentration $3.5\times10^{-3}$ of Li vacancies.

Magnetic polarons are commonly observed in magnetic semiconductors where they have been extensively studied (for a review, see [23]), including in Fe-based magnetic semiconductors [24-25]. In $LiFePO_4$, the magnetic polarons have been studied in [26-27], and they can be detected by the analysis of the magnetic properties (Fig. 3). For that purpose, we note that the $Fe^{2+}$ ions that may be coupled ferromagnetically to the $Fe^{3+}$ ion spin are the $Fe^{2+}$ ions that have non negligible interaction with the $Fe^{3+}$ ion, *i.e.* the 8 $Fe^{2+}$ ions with spin $S$=2 (four coupled by $J_1$, two by $J_2$, two by $J_b$, according to the notations of section 2), each of them carrying a spin $S$=2. Since the spin of the central $Fe^{3+}$ ion is $S$=5/2, we expect the macro-spin associated to the polaron to be $S_{pol}$=5/2 + 8*2=18.5, hence a magnetic moment $\mu_{pol}=g\mu_B S_{pol}$=37 $\mu_B$. This large spin value increases the magnetic susceptibility below the spin ordering temperature for the cluster, and is then responsible for an increase of the effective magnetic moment $\mu_{eff}$ deduced from the Curie Weiss law below 300 K. Instead of the intrinsic value $\mu_{eff}$ =4.9 $\mu_B$ met for insulating samples, we find $\mu_{eff}$ that is larger. This is illustrated in Fig. 4 for a sample of submicron sized particles large enough so that surface effects are negligible (they are discussed in the next section). The value of the concentration $c$ of magnetic polarons can be deduced from the deviation of $\mu_{eff}$ from 4.9 $\mu_B$ using the formula [27-28]

$$3k_BC = (1\text{-}c)[\mu(Fe^{3+})]^2 + c(\mu_{pol})^2 - 8c[\mu(Fe^{2+})]^2, \quad (3)$$

with $C$ the Curie constant. We have determined that the value of $c$ deduced from Eq. (3) is $c$=3.5×10$^{-3}$ [26-27]. This value is in quantitative agreement with the value determined form the analysis of the electronic conductivity of this sample, assuming that this conductivity is due to the hopping of the polaron, with an activation energy $E_a$ determined by the motional enthalpy of the $Li^+$ vacancies rather than by the time $\tau_h$ of the electron transfer from an $Fe^{2+}$ ion to a $Fe^{3+}$ ion. The analyses of the transport and the magnetic properties are then fully self-consistent [26-27].

*3.4. Surface effects*

For nanoparticles, the fraction (1-$y$) of iron ions in the surface layer is not negligible, and we found that this contribution is different from that of the bulk, and not the same before and after carbon coating. Before carbon coating, TEM experiments show that particles free of impurities and defects, and well crystallized in the bulk, are always surrounded with a 3 nm-thick layer that is strongly disordered. The response of the magnetic moments of the iron ions is thus different for the ions in the bulk and the ions in the surface layer. Therefore, one has to add to the bulk contribution to the magnetic susceptibility

$$\chi_{bulk}(T) = yC_0/(T+\theta_0), \quad (4)$$

the contribution coming from the iron ions inside the surface layer. We found that this contribution satisfies the Curie law, so that $\chi(T)$ takes the form

$$\chi(T)= yC_0/(T+\theta_0) +(1\text{-}y)C'/T; \ (T\geq 100 \text{ K}). \quad (5a)$$

There are two fitting parameters, the fraction y of iron ions in the bulk, and $C'$. We have shown that the solution for the set ($y$, $C'$) is unique, and for particles with diameter 40 nm, which is the case chosen as an example for the data reported in Fig. 5, it is [29]

$$y=0.89, \ C'=0.37 \text{ emuK/mol}. \quad (5b)$$

It should be noticed that the contribution of the core region to the magnetic susceptibility reduced to the Curie-Weiss expression only in the paramagnetic regime. On another hand, the absence of spin correlations evidenced by the Curie law implies that, at any temperature, including below $T_N$

$$\chi(T) - \chi_{bulk}(T) = (1\text{-}y)C'/T \quad \forall T, \quad (6)$$

which has been verified [29].

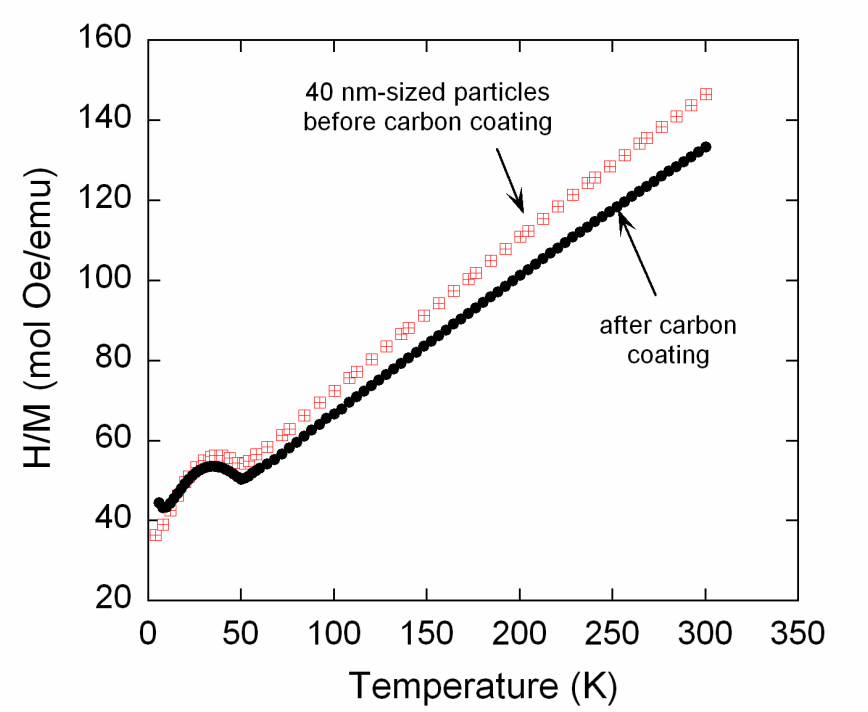


**Figure 5**. Inverse of the magnetic susceptibility of $LiFePO_4$ (particle size 40 nm) before and after carbon coating, as a function of temperature.

This behavior at low temperature allows us to distinguish between the increase of the effective moment due to the magnetic polarons investigated in the previous section (see Fig. 4) and surface effects (Fig. 5), since the polarons care spin-frozen at low temperature and do not give a Curie contribution to the susceptibility. The value of $y$ is self-consistent with the ratio $N_S/N_B$, with $N_S$ the number of iron ions in the 3 nm-thick surface-layer and $N_B$ the number of iron ions in the core region of a spherical particle of 40 nm in diameter. The value of $C'$, however, was not necessarily expected, as it corresponds to a spin $S$=1/2, implying that iron in the surface layer of uncoated particles is $Fe^{3+}$ in the low spin state.

On this example, the magnetic properties of uncoated particles have revealed important properties. First of all, the iron in the surface layer is trivalent. A significant amount of $Fe^{3+}$ is systematically detected in $LiFePO_4$ by Mössbauer experiments although they do not give any information on their location [30]. The magnetic properties are the first evidence that these $Fe^{3+}$ ions are localized in the surface layer. In addition, the analysis of $\chi(T)$ has shown that the $Fe^{3+}$ ions are uncorrelated, since there contribution is a Curie law $C'/T$ with vanishing Curie-Weiss temperature (at least down to 10 K). This is the evidence for important frustration of the magnetic interactions in the surface layer: the de-correlation of the magnetic spins is the translation on the magnetic properties of the structural disorder that affects the surface layer. Finally, the $Fe^{3+}$ ions are in the low-spin state. Remember that a free ion, i.e. ion not submitted to the crystal field, is always in the high spin state due to the Hund's rule. The low-spin state is then signature that the crystal field is big enough to break the Hund's rule. This is another signature of an important structural disorder that enhances crystal-field effects in the surface layer.

The fact that the iron ions are in the trivalent state means that the surface layer has been delithiated. After this result has been published in [29], we have made further investigations to understand the origin of this effect, and we have shown that this is due to the surface reactivity with $H_2O$ [31]. The study of the degradation of the particles upon exposure to moisture has shown that the surface layer is completely delithiated very fast, but after that, no further delithiation is observed at the scale of few days because the $FePO_4$ surface layer is waterproof and protects the core [31]. The same magnetic analysis has been performed on lamellar compounds, and they have shown that the exposure to moisture induces a delithiation over a thickness of 10 nm in that case, larger than the 3 nm in $LiFePO_4$ [32], so that the lamellar compounds are more sensitive to moisture than olive samples.

For carbon-coated particles, the inverse of the magnetic susceptibility as a function of temperature of coated particles is reported in Fig. 5, together with that of the same particles before carbon coating, for comparison. The magnetic response of the coated particles is closer to the result predicted for intrinsic $LiFePO_4$ with, however, an effective moment 5.02 $\mu_B$ still slightly larger than the theoretical value 4.90 $\mu_B$. Since $Fe^{3+}$ in the high-spin state is 5/2, its effective moment is 5.92, and we note that

$$y(4.9)^2+(1-y)(5.92)^2=(5.02)^2, \quad (7)$$

which means that the excess in magnetic moment with respect to the theoretical value is entirely attributable to the conversion of $Fe^{3+}$($S$=1/2) in $Fe^{3+}$($S$=5/2) in the surface layer. This is the evidence that the Hund's rule is no longer violated, so that the crystal field effects inside the surface layer are reduced. Therefore, we conclude that the disorder of the surface layer has disappeared in the coating process [29]. More recently, in-situ HRTEM experiments confirmed this result, and gave enlightenment to this phenomenon [33]. Note the surface layer is now well crystallized, but still the iron ions in it are in the $Fe^{3+}$ configuration, giving evidence that the layer is delithiated, so that the carbon layer is not a protection against exposure to moisture. Again, this has been confirmed by other characterization means [29].

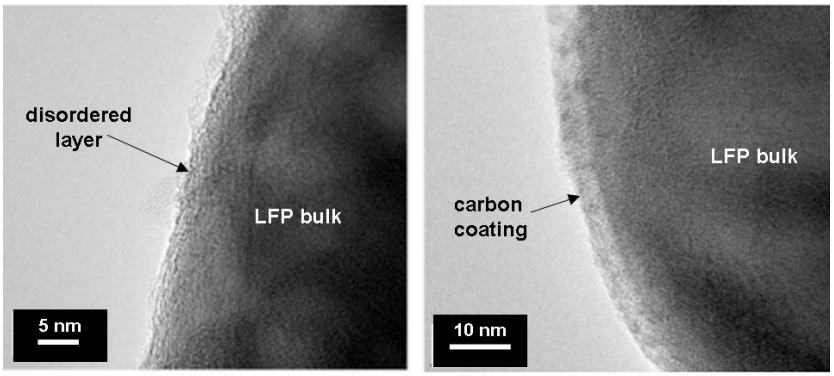


**Figure 6**. TEM images of the surface of $LiFePO_4$ particles before carbon coating (left) and after carbon coating (right). Note the granular aspect of surface before carbon coating. The lighter part surrounding the particle on the right side is the carbon layer, deposited on a surface that is less disordered.

Moreover, we have noticed that, after the carbon coating, the disordered surface layer of $LiFePO_4$ has been crystallized [40]. We have shown that this is an annealing effect of the heating process at 650-700 °C during the carbon coating process: another benefic side effect. The combination of these effects of the carbon coating process implies that the coating of $LiFePO_4$ is mandatory. All these effects are observed for particles of any size, at least in the range $d \geq 35$ nm where it has been tested: after the coating, the $LiFePO_4$ particles are well crystallized, free of impurities, the disorder surface layer has disappeared, and they are covered with a 3 nm thick layer of conductive carbon. This is illustrated in Fig. 6. Note the benefit in the case of nanoparticles is much more important than in the case of bigger particles: a disordered surface layer that is 3 nm thick involves a negligible part of micron-sized particle, but an important part of a particle of size $d$=35 nm.

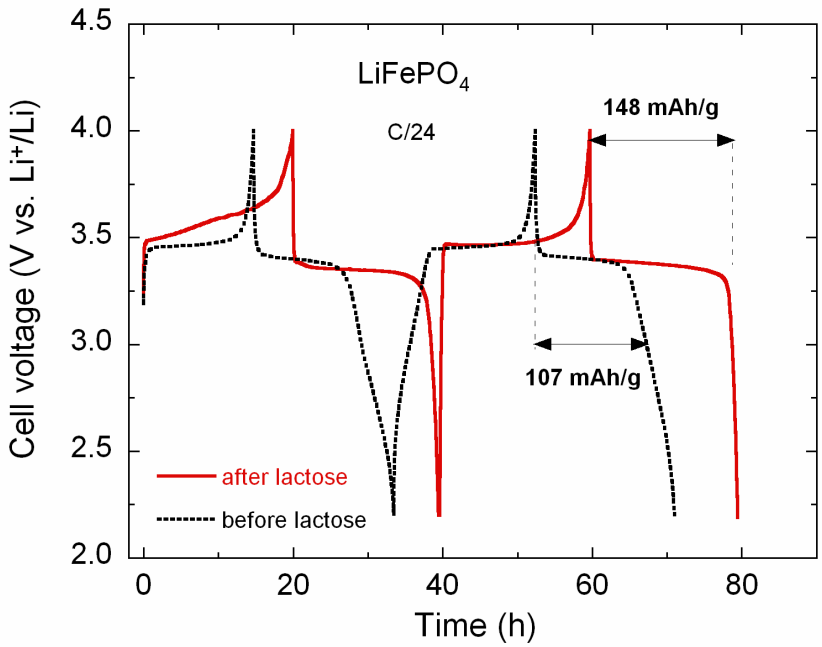


**Figure 7**. Charge–discharge voltage profiles of $LiFePO_4$/$LiPF_6$-EC-DEC/Li cells with the cathode prepared with the 40 nm sized $LiFePO_4$ particles before carbon coating and after carbon-coating.

The capacity retention of a cathode active material is strongly dependent of the surface chemistry of the particles of the insertion material, which are always covered by surface films limiting the Li-ion migration and their charge transfer across the active interface [34]. That is true for any cathode element, and $LiFePO_4$ is no exception. Figure 7 shows the charge–discharge voltage profiles of $LiFePO_4$/1 mol $L^{-1}$ $LiPF_6$-EC-DEC/Li cells at C/24 rate with the cathode prepared with the 40 nm sized $LiFePO_4$ particles before carbon coating and after carbon-coating [35]. The plateau characteristic of the two-phase region is recovered after carbon-coating as it can be seen in Fig. 7 for particles of size $d$=40 nm, which shows that the two-phase insertion/deinsertion process is recovered even for such small particles. Discharge capacity of 148 mAh/g is provided by C-$LiFePO_4$ after carbon deposit by the lactose method. The modified Peukert plots measured upon discharge are reported in Fig. 8. These

results show clearly the capacity enhancement with a carbon deposit of *ca.* 3 nm ob the surface of primary particles (*d*=40 nm). Note the performance of the cell with C-$LiFePO_4$ should be slightly improved at high C-rates with respect to the laboratory cell presented in the figures, when it will be manufactured with the industrial optimized process for 18650-type cell [2].

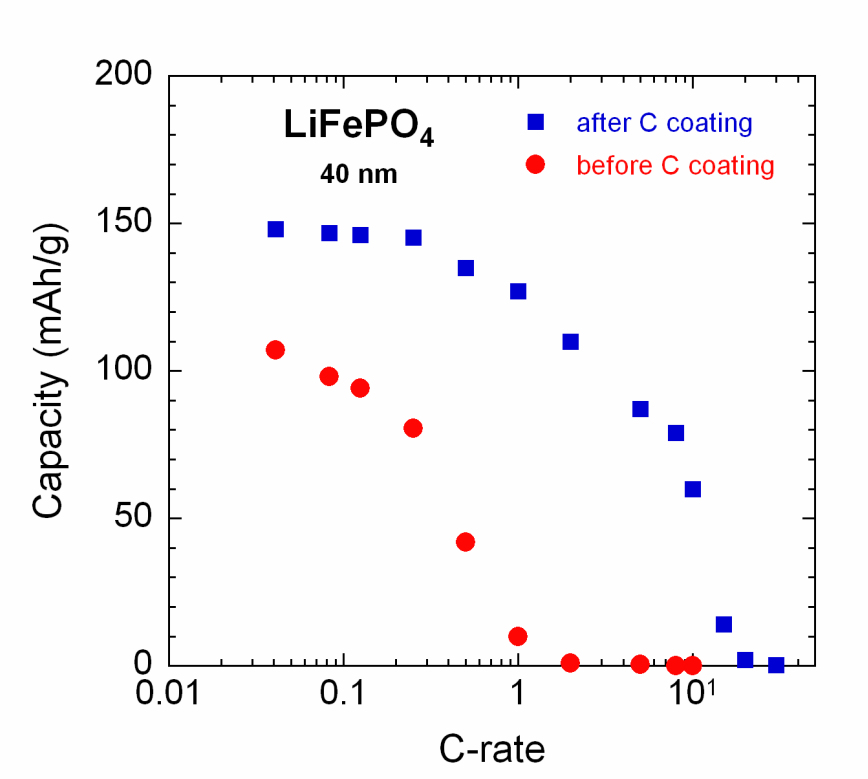


**Figure 8**. Modified Peukert (discharge) plots of the $LiFePO_4/LiPF_6$ in EC-DEC/Li cells with cathode material before carbon coating and after carbon-coating.

## 4. CONCLUSIONS

Magnetic experiments have been as been as powerful to characterize $LiFePO_4$ as in the case of lamellar compounds. They have played a key role to identify the impurities, and quantify their amount in relation to the synthesis parameters. Owing to this correlation between synthesis and magnetic properties, it was possible to get rid of all of the impurities that damaged the electrochemical properties of this cathode element. The magnetic experiments have also allowed the determination of the concentration of the Li-vacancies, showing that it is the main defect in this material; it has been confirmed later on by the calculations of the electronic structure. Finally, the magnetic experiments proved also efficient to characterize the surface layer, its sensitivity to moisture, and the annealing effect on its degree of disorder. Since all the cathode elements for Li-ion batteries are oxides of transition metals, the same analysis will prove relevant to their characterization as well, so that we believe they will pay a major role in the research and development on these ionic compounds for years to come.

**References**


1. The 85-kWh battery that powers the Tesla S Sedan electric car insures autonomy of 300 miles per charge for instance. This car accelerates to 60 mph in 4.4 seconds.
2. K. Zaghib, M. Dontigny, A. Guerfi, P. Charest, I. Rodrigues, A. Mauger and C. M. Julien, *J. Power Sources,* 196 (2011) 3949
3. K. Padhi, K. S. Nanjundaswamy and J. B. Goodenough, *J. Electrochem. Soc*., 144 (1997) 1188
4. N. Ravet, Y. Chouinard, J. F. Magnan, S. Besner, M. Gauthier and M. Armand, *J. Power Sources,* 97 (2001) 503
5. X. Zhang, C. Julien, A. Mauger and F. Gendron, *Solid Stat. Ionics,* 188 (2011) 148
6. C. M. Julien, A. Mauger and K. Zaghib, *J. Mater. Chem.,* 21 (2011) 9955
7. K. Zaghib, A. Mauger, J.B. Goodenough, F. Gendron and C. M Julien, *Encyclopedia of Electrochemical Power Sources*, Elsevier Science, Amsterdam (2009)
8. R. P. Santorro and R. E. Newnham, *Acta Crystallogr*., 22 (1967), p. 344
9. R. P. Santorro, D. J. Segal and R. E. Newnham, *J. Phys. Chem. Solids,* 27 (1966) 1192
10. D. Dai, H.-J. Koo, X. Rocquefelte and S. Jobic, *Inorg. Chem.,* 44 (2005) 2407
11. J. M. Mays, *Phys. Rev*., 131 (1963) 38
12. C. M. Julien, A. Mauger, A. Ait-Salah, M. Massot, F. Gendron and K. Zaghib, *Ionics,* 13 (2007) 395
13. A. Mauger, F. Gendron and C. M. Julien, *J. Alloys Compds*, 520 (2012) 42
14. P. Jozwiak, J. Garbarkczyk, F. Gendron, A. Mauger and C. M. Julien, *J. Non-Cryst. Solids,* 354 (2008) 1915
15. P. Jozwiak, J. Garbarkczyk, A. Mauger, F. Gendron and C. M. Julien, *Extented Abstracts of the MRS Fall Meeting Solid State Ionics,* 0972 (2006) 703.
16. N. Ravet, M. Gauthier, K. Zaghib, A. Mauger, J. B. Goodenough, F. Gendron and C. M. Julien, *Chem. Mater*., 19 (2007) 2595
17. P. S. Herle, B. Ellis, N. Coombs and L. F. Nazar, *Nat. Mater*., 3 (2004) 147
18. A. Ait-Salah, A. Mauger, C. M. Julien and F. Gendron, *Mater. Sci. Eng. B,* 129 (2006) 232
19. A. Ait-Salah, J. Dodd, A. Mauger, R. Yazami, F. Gendron and C. M. Julien, *Z. Allg. Inorg. Chem.*, 632 (2006) 1692
20. K. Zaghib, N. Ravet, M. Gauthier, F. Gendron, A. Mauger, J. B. Goodenough and C. M. Julien, *J. Power Sources,* 163 (2006) 560
21. P. Axmann, C. Stinner, G. Arnold and M. Wohlfahrt-Mehrens, private communication
22. F. Zhou, M. Cococcioni, K. Kang and G. Ceder, *Electrochem. Commun*., 6 (2004) 1144
23. A. Mauger and C. Godart, *Phys. Reports,* 151 (1986) 51
24. T. Testelin, R. Rigaux, A. Mauger and A. Mycielski, *Phys. Rev. B,* 46 (1992) 2193
25. D. Scalbert, J. A. Gaj, J. Cernogora and C. Benoît à la Guillaume, *Phys. Rev. Lett*., 62 (1989) 2865
26. K. Zaghib, A. Mauger, J. B. Goodenough, F. Gendron and C. M. Julien, *Chem. Mater*., 19 (2007) 3740
27. A. Mauger, K. Zaghib, F. Gendron and C. M. Julien, *Ionics,* 14 (2008) 209
28. K. Zaghib, A. Mauger, F. Gendron and C. M. Julien, *Solid State Ionics,* 179 (2008) 16
29. K. Zaghib, M. Dontigny, P. Charest, J. F. Labrecque, A. Guerfi, M. Kopec, A. Mauger, F. Gendron and C. M. Julien, *J. Power Sources,* 195 (2010) 8280
30. A. S. Andersson, B. Kalska, L. Häggström and J. O. Thomas, *Solid State Ionics*, 130 (2000) 41
31. K. Zaghib, M. Dontigny, P. Charest, J.F. Labrecque, A. Guerfi, M. Kopek, A. Mauger, F. Gendron and C. M. Julien, *J. Power Sources*, 185 (2008) 698
32. X. Zhang, W.J. Jiang, X.P. Zhu, A. Mauger, Q. Lu and C. M. Julien, *J. Power Sources,* 196 (2011) 5102
33. M. L. Trudeau, D. Laul, R. Veillette, A.M. Serventi, K. Zaghib, A. Mauger and C. M. Julien, *J. Power Sources,* 196 (2011) 7383

34. D. Aurbach, K. Gamolsky, B. Markovsky, G. Salitra, Y. Gofer, U. Heider, R. Oesten and M. Schmidt, *J. Electrochem. Soc.*, 147 (2000) 1322
35. K. Zaghib, A. Mauger, F. Gendron and C. M. Julien, *Chem. Mater.*, 20 (2008) 462